Chemical Engineering Journal 454 (2023) 140261

Contents lists available at ScienceDirect

Chemical Engineering Journal

journal homepage: www.elsevier.com/locate/cej

Breakage-resistant hydrogel electrode enables ultrahigh mechanical reliability for triboelectric nanogenerators

Rui Li [a,b], Zhenyu Xu [b,c], Long Li [a,b], Junjie Wei [b,*], Wenqin Wang [a,*], Zejun Yan [d], Tao Chen [b,c,*]

[a] School of Materials Science and Chemical Engineering, Ningbo University, Ningbo 315211, China
[b] Key Laboratory of Marine Materials and Related Technologies, Zhejiang Key Laboratory of Marine Materials and Protective Technologies, Ningbo Institute of Materials Technology and Engineering, Chinese Academy of Sciences, Ningbo 315201, China
[c] School of Chemical Sciences, University of Chinese Academy of Sciences, Beijing 100049, China
[d] Department of Urology & Nephrology, Ningbo First Hospital, The Affiliated Hospital of ZheJiang University. 59, Liuting Street, Ningbo 315010, China

ARTICLE INFO

Keywords:
Breakage-resistance
Hydrogel electrodes
Mechanical reliability
Triboelectric nanogenerators
Hofmeister effect

ABSTRACT

Hydrogel based triboelectric nanogenerators (H-TENGs) are deemed as one of most promising flexible energy harvesting and self-powered systems due to its multifunctionality, but the poor mechanical properties of hydrogel electrode bring a major risk of shortening the service life of H-TENGs in case of huge physical impact. Herein, a durable conductive hydrogel electrode with breakage-resistant capacity is developed utilizing the Hofmeister effect on starch polymers through solvent-exchange strategy. Owing to bundled starch chains within hydrogel, the breakage-resistant hydrogel electrode possesses excellent mechanical reliability, including outstanding modulus, fracture energy, anti-puncture capacity and long-term stability. Furthermore, the reliable hydrogel electrode endows triboelectric nanogenerator with good electrical output performances and superb damage immunity, prolonging its service life under accidental physical impact. More significantly, this fabricated triboelectric nanogenerator shows great potential in high-impact application. This investigation offers a versatile and effective way to design next generation hydrogel-based triboelectric nanogenerator with superior damage immunity and long-service life.

1. Introduction

Since Wang et al [1] first proposed the concept of triboelectric nanogenerators (TENGs) in 2012, it has made rapid development and achieved various breakthroughs because of its attractive advantages of simple fabrication, multiple structures, cost-effectiveness, and great efficiency at low operating frequencies [2,3]. As a promising technology in the field of energy harvesting and self-powered systems, TENGs can convert various forms of mechanical energy into electrical energy based on the combination of contact electrification and electrostatic induction [4–7]. Nowadays, TENGs have been widely applied in various intelligent fields, such as biomedical/implantable electronics [8] sports detection [9], human-machine interaction [10], real-time event assistance [11], intelligent library [12], security protection [13], water harvesting [14] and so on [15–18], Among numerous electrode materials (e.g. metal materials, carbon materials, polymer materials and MOFs) [19–21] playing a crucial role in TENGs, conductive hydrogel electrode has attracted increasing attention due to unique properties [22]. Benefitting from their tunable ionic conductivity and fascinating modifiability, hydrogel electrodes exhibit great potential to improve the comprehensive performance and broaden their application by endowing TENGs with multifunctionality[23]. For example, Sun et al [24] reported an anti-freezing and anti-drying organogel electrode through a convenient solvent-exchange strategy, which greatly improve the environmental tolerance and the harvest energy efficiency of TENGs under extreme temperatures (-60 °C to 60 °C). Similarly, Wang's group [25] fabricated a flexible TENG by employing MXene/PVA hydrogel electrode, this hydrogel electrode not only promotes the stretchability of TENG, but also induced an extra output via a streaming vibration potential mechanism. In addition, compared to other electrode materials, hydrogel electrodes possess excellent properties of large stretchability [26], high transparency [27], good biocompatibility [28] and environmental friendliness [29].

Although hydrogel based TENGs (H-TENGs) have made great

* Corresponding authors at: Key Laboratory of Marine Materials and Related Technologies, Zhejiang Key Laboratory of Marine Materials and Protective Technologies, Ningbo Institute of Materials Technology and Engineering, Chinese Academy of Sciences, Ningbo 315201, China (T. Chen).
E-mail addresses: weijunjie@nimte.ac.cn (J. Wei), wangwenqin@nbu.edu.cn (W. Wang), tao.chen@nimte.ac.cn (T. Chen).

https://doi.org/10.1016/j.cej.2022.140261
Received 11 August 2022; Received in revised form 17 October 2022; Accepted 5 November 2022
Available online 11 November 2022

progress in improving electrical output performances and achieving multifunctionality, there is still a major concern about its physical reliability during the long-term operation. Hydrogel electrode with bad mechanical strength is easier to be damaged physically by unpredictable external force (such as strong impact, puncture and multiple cuts), which greatly shorten the service life and restrain the development potential of H-TENGs. Thus, it is of great significance to solve the physical damage of H-TENGs for improving their physical reliability and prolonging their life. To date, the main method to solve this problem is to design self-healing hydrogel electrodes by introducing dynamic bonds [30,31], expecting that the performance of damaged H-TENG can be recovered after self-healing treatment. For example, Wang's group developed a self-healing conductive hydrogel electrode for wearable H-TENGs utilizing the thermally reversible sol-gel transition [32] and it exhibited a high self-healing efficiency of 85 % at 60 °C. Unfortunately, there exist some shortcomings in practice for the self-healing strategy, such as long healing time, harsh healing conditions, low healing efficiency, narrow and irregular broken section. Therefore, how to effectively extending its service life remains an urgent challenge for H-TENGs.

Actually, the distressing short-life of H-TENGs in case of mechanical damage is mainly caused by the poor mechanical strength of hydrogel electrodes. Thus, enhancing the intrinsic mechanical strength of hydrogel electrodes contributes to improving the physical reliability and prolonging the service life of H-TENGs fundamentally. Inspired by this, herein, we developed a simple and efficient method for preparing breakage-resistant conductive hydrogel (BRC hydrogel) with ultrahigh mechanical reliability via solvent-exchange strategy (Fig. 1a). Employing this BRC hydrogel as electrode material, an excellent H-TENG with high mechanical safety and long life was fabricated successfully. Benefiting from the BCR hydrogel electrode, this reliable H-TENG showed satisfactory performance of resisting physical damage, and even can be used for real-time monitoring high-impact movements, such as running (Fig. 1c).

2. Materials and methods

2.1. Materials

Starch, Hydroxyethyl mathacrylate (HEMA), Dimethyl sulfoxide (DMSO), Sodium citrate (NaCit), N, N′ -Methylenebis(acrylamide) (MBAA) were purchased from Shanghai Aladdin Biochemical Technoligy Co., Ltd. Acrylamide (AAm) was purchased from the Sinopharm Chemical Reagent Co., Ltd. N, N′ -Bis(acryloyl)cystamine (BACA) was purchased from Shanghai Macklin Biochemical Technoligy Co., Ltd. Ammonium persulfate (APS) and N, N, N′, N′ -Tetramethylethylenediamine (TEMED) were purchased from Aladdin Chemistry Co., Ltd. Deionized water was used in all experiments. VHB^{TM} 4905 was obtained from 3 M Corporation. All chemicals were used as received.

2.2. Preparation of organogel

Typically, starch (0.8 g) was added to DMSO (7.2 mL) and then stirred intensely for at least 24 h at room temperature. After starch was completely dissolved, HEMA (2.0 mL) and BACA (0.02 g) were added to the mixed liquid and stirred for 1.5 h. Then, APS (0.0667 g) and TEMED (100 μL) were dissolved in the above mixed solution, and the final solution was injected into glass cell that was separated with a 1 mm-thick Polydimethylsiloxane (PDMS) spacer through a needle tube. After fully polymerization at 30 °C for 48 h, the organogel was obtained.

2.3. Preparation of breakage-resistant conductive hydrogel (BRC hydrogel)

BRC hydrogel was prepared through a simple solvent-exchange strategy. Typically, the prepared organogel was soaked in 1 M sodium citrate solution for 24 h, and then the BRC hydrogel was obtained successfully.

2.4. Fabrication of BRC hydrogel based triboelectric nanogenerator:

The breakage-resistant conductive hydrogel based triboelectric

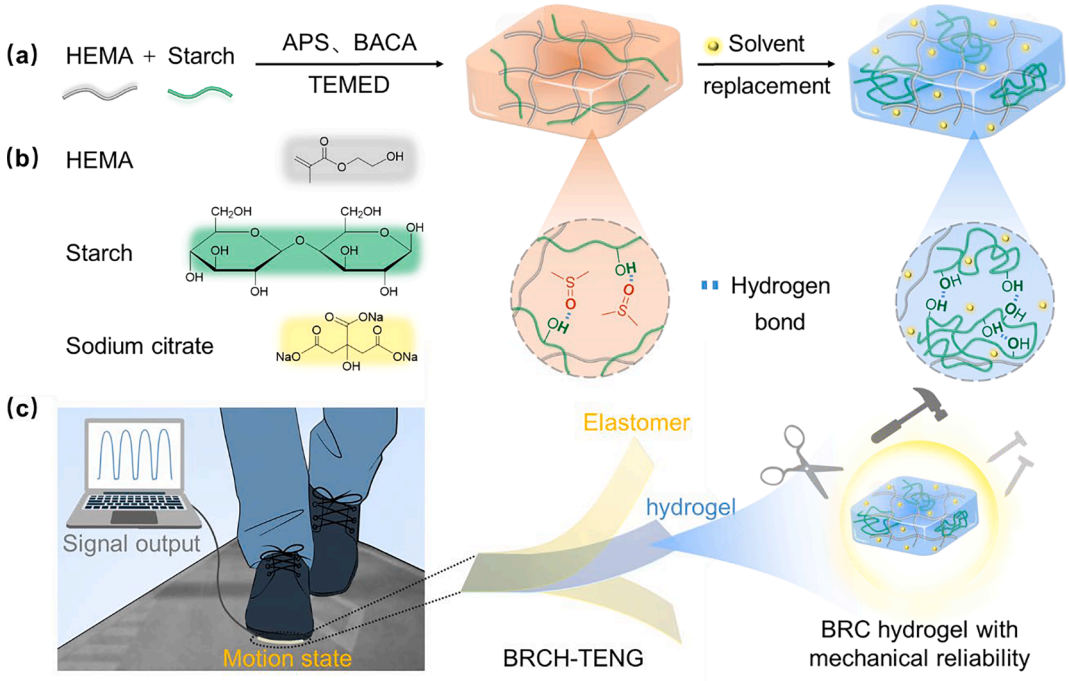

Fig. 1. Breakage-resistant conductive hydrogel and its potential application in mechanical-reliable TENG. (a) Schematic illustration of preparing the BRC hydrogel. (b) Key components of precursor solution. (c) Architecture, mechanical reliability and its self-power sensing application of the BRC hydrogel based TENG.

nanogenerator (BRCH-TENG) was fabricated by sandwiching the BRCH hydrogel and copper foil between two pieces of VHB^{TM} 4905 elastomer. The thickness of the BRCH hydrogel and elastomer were 0.8 mm and 1 mm, respectively.

2.5. Mechanical tests

The Zwick Roell Z1.0 universal material testing machine (Zwick, Germany) was employed for mechanical tests. For tensile test, the organogel or the hydrogel samples were cut into 10 × 30 mm^2. The speed of tensile test was 50 mm/min. The strain was calculated as $(l\text{-}l_0)/l_0 \times 100$ %, where l_0 was the initial length, l was the real-time length. The modulus was determined as the slope of stress-strain curve in the strain range of 5–15 %. The toughness was characterized as the area surrounded by the stress-strain curve. For compressive test, the samples were cylindrical, and the diameters of samples were 8 mm, the heights were 4 mm. The speed of compression test was 50 mm/min. For fracture energy test, an unnotched sample and a notched sample (with a 3 mm gap in the middle) were stretched under the same condition. The size of sample is 10 × 30 mm^2. The fracture energy (Γ) was calculated as $\Gamma = A/(d{\cdot}l)$, where A was the area surrounded by force-displacement curve of the unnotched sample (Note that the displacement is the maximum displacement of the notched sample), d was the thickness of the samples, l was the width of the samples. For puncture force strength test, the sample (60×60 mm^2) was punctured by a needle with the tip of 0.3 mm at the speed of 50 mm/min.

2.6. Performance characterization of BRCH-TENG

The Keithley 6514 electrometer was employed for the performances (including I_{sc}, V_{oc} and Q_{sc}) of BRCH-TENG. The output signals were treated with baseline correction in the walking test. The resistors with different resistance values are connected in the circuit to measure different I_{sc} and V_{oc} in the output power density measurement.

3. Results and discussion

The breakage-resistant conductive hydrogel was synthesized by a simple solvent-exchange strategy as illustrated in Fig. 1a. Firstly, the homogeneous precursor solution was prepared by dissolving starch, monomer (Hydroxyethyl mathacrylate, HEMA), crosslinker (N, N′ -Bis (acryloyl)cystamine, BACA), thermal initiator (Ammonium persulfate, APS), accelerator (N, N, N′, N′ -Tetramethylethylenediamine, TEMED) in Dimethyl sulfoxide (DMSO) under continuous magnetic stirring. Then a transparent organogel was obtained by thermal-initiation polymerization at 30 °C for 48 h. Finally, the organogel was immersed in sodium citrate (NaCit) solution, and the desired breakage-resistant conductive hydrogel was obtained successfully after fully replacement due to the Hofmeister effect. Notably, starch was chosen as the component of the BRC hydrogel due to its abundant hydroxyl group and remarkable Hofmeister effect on ions, which is crucial to improving its mechanical properties. Besides, most of the components in the BCR hydrogel are non-toxic, and even biodegradable, ensuring that the BCR hydrogel were biocompatible and eco-friendly.

Starch is insoluble in water because of the strong hydrogen bonds between polymer chains, but DMSO can destroy these hydrogen bonds and dissolve starch efficiently. Thus, the organogel can be prepared successfully in DMSO solvent, and there are abundant hydrogen bonds between S═O of DMSO and H—O of starch polymers, which maintain the stability of starch chains in the organogel. After soaking treatment, the DMSO was fully replaced by NaCit solution, and the starch chains tend to fold and curl under the Hofmeister effect of kosmotropes (Na^+, $citrate^-$). Finally, the bundling starch chains were aggregated and stabilized attributed to the formation of new hydrogel bonds between inter- or/and intra-molecules. Hydrophobic chain association plays the role of physically crosslinked domains, which increase the polymer chain density and chain friction and improve the hydrogel's mechanical properties, including excellent breakage resistance. This process was proved by the Fourier transform infrared (FTIR) test. As shown in Fig. 2a, the broad characteristic peak ascribed to the O—H stretching vibration of starch polymer was found at 3358 cm^{-1} when the organogel was fully soaked in deionized water. However, after soaking treatment with 0.5 M and 1.0 M NaCit solution, the peak position of O—H stretching vibration shifts to lower wavenumbers of 3336 cm^{-1} and 3313 cm^{-1}, respectively, indicating that there is an enhanced hydrogen bonding interaction among bundled starch polymers. Besides, the peaks at 1056 cm^{-1} and 1013 cm^{-1} are attributable to the ordered region and amorphous region of starch, and the absorbance ratio of 1056 cm^{-1}/1013 cm^{-1} can be used to evaluate its crystallinity [33]. It is significant that the absorbance ratio of characteristic peaks increased remarkably when the concentration of NaCit solution increased from 0 M to 1.0 M, suggesting the increase of the crystallinity of starch molecules due to the formation of hydrogel bonds between inter- or/and intra-molecules under Hofmeister effect. The new peak occurred at 1580 cm^{-1}, representing the symmetric vibration of the carboxylate ion (i.e. $citrate^-$) [34], confirmed the NaCit was introduced into the hydrogel system successfully.

The change in transmittance of gel was also verified the above mechanism from the side. As shown in Fig. 2b, the transmittance of organogel was about 87 % in the visible wavelengths, while the value dropped below 70 % after solvent-exchange treatment. This is because the Hofmeister effect-induced chain entanglement leads to the formation of hydrophobic zone and the microphase separation within BRC hydrogel. The porous structure of hydrogels was observed using scanning electron microscope (SEM). As shown in Fig. 2d, the pore size of BRC hydrogel is ~4 μm, far smaller than that of the hydrogel treated by deionized water (~12 μm, Fig. 2c). The smaller pores for BRC hydrogel demonstrated that the starch chain interactions induced by Hofmeister effect increased the crosslink density, which contribute to improve the mechanical properties. As visual evidences, some experiments were carried out in this investigation. For example, the BRC hydrogel can be rolled, knotted and stretched, exhibiting high flexibility and stretchability (Fig. S1). More importantly, the BRC hydrogel possesses excellent penetration resistance, there is no any breakage under the puncture of a sharp steel needle (Fig. 2e). Besides, the BRC hydrogel string can readily lift a weight of 1 kg (Fig. 2f), revealing superb mechanical strength. In addition to the enhancement of mechanical properties, the solvent-exchange process also endows the hydrogel with large amounts of ions, leading to a good ionic conductivity. As shown in Fig. 2g and Fig. S2, due to the competitive effect of ion concentration and chain crosslinking density, the BRC hydrogel reached the highest ionic conductivity of 6.02 mS/cm when the concentration of NaCit solution is 1 M and the content of starch is 8 wt%. Thus, 1 M was selected as the concentration of NaCit solution in the following study. This satisfactory ionic conductivity enables it to work as electrode material for flexible TENG.

Some mechanical measurements were carried out to systematically evaluate the enhancement effect of solvent-exchange strategy. For comparison, three types of gels (organogel without solvent-exchange, hydrogel soaking with NaCit solution, hydrogel soaking with deionized water) were prepared in these measurements, and they were denoted as "S_xD", "S_xN" and "S_xW" (the value of "x" means the mass fraction of starch), respectively. As shown in Fig. 3a, the tensile stress at fracture of the BRC hydrogel is more than 0.7 MPa due to the increased chain density and chain friction, far greater than that of the organogel (~0.018 MPa). Although the chain density and chain friction have reached a high value when the starch content is 6 wt%, there is still a small increase in tensile properties when the starch content increased from 6 wt% to 10 wt%, and the BRC hydrogel reached the highest tensile strength of 0.86 MPa when starch content is 10 wt%. The similar phenomenon can be observed from the compression test. Compared to the organogel without solvent-exchange treatment, the compressive

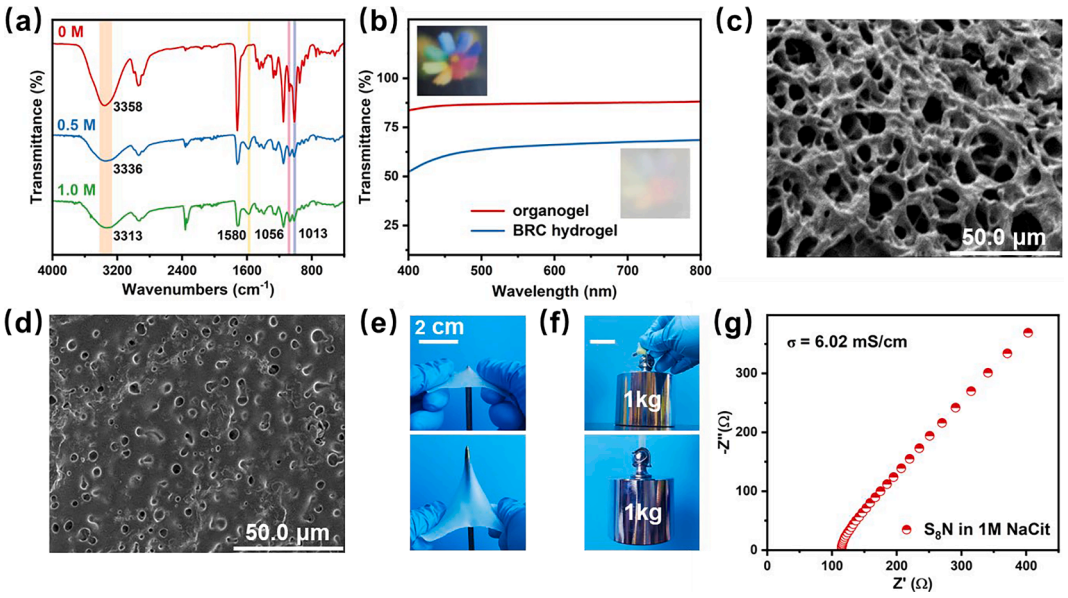

Fig. 2. Characterization of the BRC hydrogel. (a) FTIR spectra of starch-based hydrogels after different treatment. (b) Transmittance of organogel and BRC hydrogel with 8 wt% starch. (c-d) SEM images of the hydrogel after solvent-exchange treatment by (c) deionized water and (d) 1 M NaCit solution. (e-f) Photographs showing the BRC hydrogel with 8 wt% starch (e) subjected to puncture by a sharp steel needle and (f) lifted a 1 kg weight. (g) Nyquist plots of the BRC hydrogel with 8 wt% starch after soaking in 1 M NaCit solution.

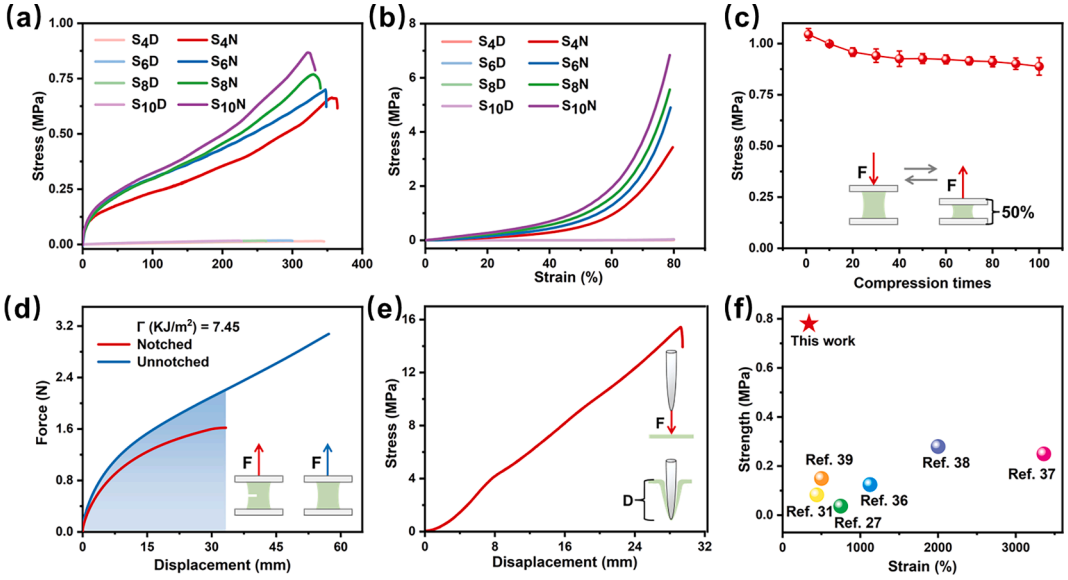

Fig. 3. Mechanical properties of the BRC hydrogel. (a) Tensile curves of the organogel and BRC hydrogel with various starch content. (b) Compression curves of the organogel and BRC hydrogel with various starch content. (c) Mechanical stability of S_8N BRC hydrogel during the 100-cycle compression tests. (d) Force–displacement curves of the notched and unnotched S_8N BRC hydrogels. (e) Puncture curve of S_8N BRC hydrogel at the speed of 50 mm/s, the diameter of the needle tip is 0.3 mm. (f) Comparison of mechanical strength for BRC hydrogel to some previously reported hydrogel electrode of H-TENGs.

strength of BRC hydrogel increased greatly, and the maximum strength even reached about 6.83 MPa at a strain of 80 % (Fig. 3b). After NaCit solvent-exchange, the biggest increment value of modulus of BRC hydrogel achieves 189 times, compared with the original organogel. Rheological characterization (Fig.S3) further proved the effectiveness of solvent replacement strategy. Besides, the BRC hydrogel exhibits good stability in the repeated compression. As shown in Fig. 3c and Fig. S4, although the compressive stress of BRC hydrogel gradually decreased during cycle compression due to the inevitable break of polymer and the irreversible destruction of network structure, it exhibited a satisfactory stability owing to its physical crosslinking network and efficient energy dissipation. And the effect of compression rate and strain on mechanical stability is negligible (Fig. S5). This stable mechanical property under continuous beat is benefit for improving the long-term stability of the BRC hydrogel based TENG. As a contrast, the mechanical properties of hydrogel treated with deionized water (S_xW) were analyzed using the same measurements, and these studies showed that the mechanical strength of hydrogel could not be increased by deionized water immersion (Fig. S6). This result confirmed again that the enhancement effect of solvent-exchange method is mainly attributed to the Hofmeister effect of NaCit solution.

In addition to the threat from continuous high-intensity work, the risk of accidental physical damages (such as cutting, tearing and puncture) can severely shorten the lifespan of hydrogel electrode and H-

TENG. Therefore, we assessed the fracture energy and anti-puncture properties of BRC hydrogel. As shown in Fig. 3d, the fracture energy was measured referring to the work reported by Suo, [35] and the BRC hydrogel (S_8N) exhibited a superior value of 7.45 kJ/m^2, about 50 times that of other samples (Fig. S7), indicating the BRC hydrogel possesses unique notch-insensitive property due to the efficient energy dissipation. The anti-puncture property was tested by puncturing with a steel needle at speed of 50 mm/min. As shown in Fig. 3e, the puncture stress of BRC hydrogel at fracture was about 15 MPa, proving the excellent reliability and safety when it suffering physical damage. Among the three types of gel, the BRC hydrogel treated with NaCit solution exhibits the best synthesized mechanical properties (Fig. S8), including modulus, strain, stress, toughness and fracture energy, which sufficiently proves the effectiveness of our solvent-exchange strategy. To our knowledge, compared to other previously reported hydrogel electrodes for H-TENGs [27,31,36–39], the BRC hydrogel shows the highest mechanical strength so far (Fig. 3f). The outstanding mechanical properties of BRC hydrogel electrode provides a higher safety guarantee for H-TENG, and helps to resist the damage caused by external force and prolong its service life.

Considering its good comprehensive performance in mechanical properties and electrical properties after solvent replacement, the S_8N BRC hydrogel was chosen to apply as electrode material for a breakage-resistant flexible TENG in the following work. Besides, the commercial VHB^{TM} elastomer was used as friction layer at the surface of TENG (Fig. S9).

As shown in Fig. 4a, the BRC hydrogel based TENG (BRCH-TENG) operated as the single-electrode mode, and its working principle could be attributed to the coupling effect of contact electrification and electrostatic induction. When the nylon film (positive tribo-material) contact with the surface of BRCH-TENG (VHB^{TM} elastomer, negative tribo-material), equivalent charges with opposite polarities were generated on the nylon film and elastomer due to triboelectric effect, but there was no electric current occurred in BRCH-TENG as the two surfaces stayed in contact with each other (Fig. 4a, step I). Once the nylon film moved away from the BRCH-TENG, the positive static charges and negative static charges on the contact surface were also separated from each other. The electrostatic charge on the surface of the insulating elastomer driven the ions in BRC hydrogel to move in order to balance the static charge. Meanwhile, due to electrostatic equilibrium, electrons flowed from the electrode to the external circuit through metal wire, forming an electric current signal (Fig. 4a, stepII). After that, a new electrostatic equilibrium was established to balance all the static electricity in the elastomer (Fig. 4a, step III). When the nylon film approached the surface of BRCH-TENG, electrons transferred from the external circuit to BRC

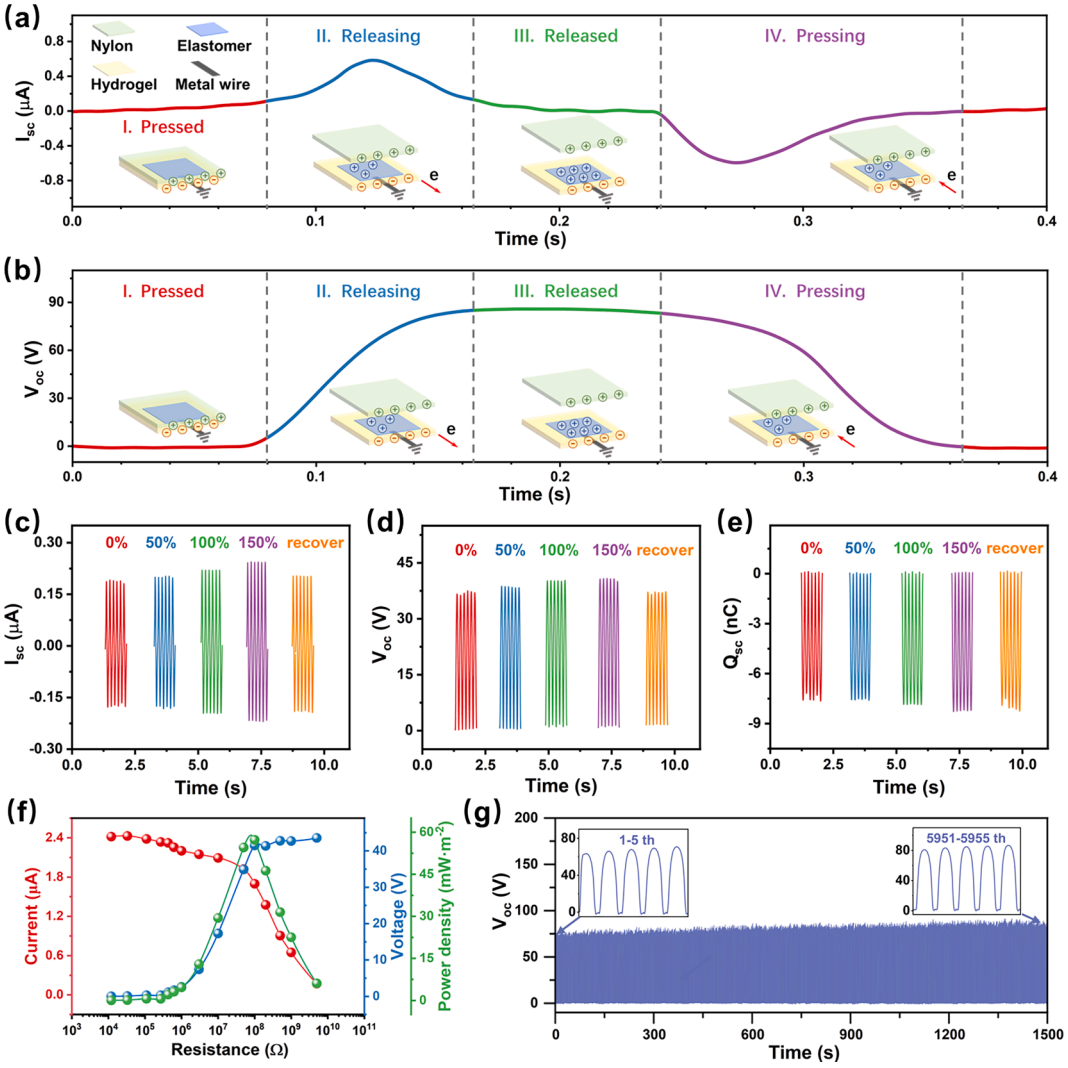

Fig. 4. Working mechanism and output characteristics of BRCH-TENG. (a) short-circuit current (I_{sc}) and (b) open-circuit voltage (V_{oc}) of the BRCH-TENG (40 mm × 40 mm) in a contact-separation cycle, the illustration show the working mechanism of the BRCH-TENG. (c) I_{sc}, (d) V_{oc} and (e) short-circuit charge quantity (Q_{sc}) of the BRCH-TENG (10 mm × 20 mm) when working at different stretching state. (f) Variation of voltage, current and power density of the BRCH-TENG (35 mm × 35 mm) with external resistances. (g) The V_{oc} of the BRCH-TENG (40 mm × 40 mm) in long-time operation (1500 s, 6000 tapping cycles).

hydrogel, resulting in a reverse electric current (Fig. 4a, stepⅣ). By repeating these contact-separation steps above, the BRCH-TENG can generate a continuous alternating electric current signal. When the single-electrode BRCH-TENG were fabricated by elastomers and hydrogel electrode with area of 40×40 mm^2, it generated a maximum short-circuit current (I_{sc}) of ~0.59 μA (Fig. 4a). During this contact-separation process, the open-circuit voltage (V_{oc}) of the BRCH-TENG also changed with the induced charges, and it reached a maximum value of ~87 V when the electrostatic equilibrium was established in the step III (Fig. 4b).

Thanks to the good stretchability of BRC hydrogel, the TENG fabricated by this BRC hydrogel electrode possesses favorable stretchability. The electrical output performances of BRCH-TENG (the size is 10 mm × 20 mm) under different stretched conditions were measured to evaluate the stretch's influence on performances. As shown in Fig. 4c, when the BRCH-TENG was stretched from 0 % to 150 %, the I_{sc} increased from 0.19 to 0.24 μA. This change in electrical output performance is mainly caused by the shape change of the BRCH-TENG. The contact area between the surface of BRCH-TENG and the nylon film increased when the BRCH-TENG was tretched, resulting in attracting more electric charges. Similarly, the V_{oc} and Q_{sc} of the BRCH-TENG also showed an increasing trend as the tensile strain increasd (Fig. 4d and e). Besides, its electrical output performances were restored to original level when the BRCH-TENG was recovered from stretched state to initial state without strain, meaning there was no obvious performance degradation in this process. This enhanced performance and recoverability is beneficial to its wearable application, which often get stretched during use. Furthermore, the electrical output performances of the BRCH-TENG at various tapping frequency were also studied. As shown in Fig. S10, the values of I_{sc}, V_{oc} slightly increased with the increasing frequency varying from 2.8 Hz to 8.3 Hz. This phenomenon is because the continuous tapping behavior was driven by a linear motor in this test, and there was a greater the accumulated charge per unit time on BRCH-TENG when the frequency increased, which lead to the enhanced electrical output performances. This ability of distinguishing and harvesting different-frequency mechanical energy makes it promising for monitoring motion and collecting energy from movement.

In order to evaluate the output power density (P) of the BRCH-TENG, its output voltage (U) and output current (I) were measured by connecting in series with external load resistances, and the output power density was calculated as the formula $P = U \times I/A$, while A was the contact area of BRCH-TENG. As shown in Fig. 4f, the power density reached a maximum value of 57.5 mW/m^2 at 100 MΩ (the size of H-TENG is 35 mm × 35 mm). Besides, the BRCH-TENG possessed excellent long-term durability in practice. As shown in Fig. 4g, there was no performance degradation for the BRCH-TENG (40 mm × 40 mm), and even a slight improvement in V_{oc} after being exposed to 6000 contact-separation cycles, which may be attributed to the improved contact between the hydrogel electrode and the elastomer resulted from the persistent external force. The superior electrical output performance and long-term durability provide a good guarantee for its practical application.

As a demonstration, a self-charging system was established by BRCH-TENG (40 mm × 40 mm), capacitor and electronics as Fig. 5a. When S_1 was closed, the BRCH-TENG could directly power serial light-emitting diodes (LEDs) by continuous beating (Fig. 5b, Video S1,2,3). When S_2 is closed, the BRCH-TENG can charge the capacitors. After charging for 180 s, the 4.7 μF capacitor, 10 μF capacitor and 47 μF capacitor were charged to ~2.8 V, ~2.5 V and ~1.0 V, respectively (Fig. 5c). When S_3 was closed, the collected energy can be used to drive electronics. The real-time charge/discharge curve of capacitor driving an electronic watch was displayed in Fig. 5d, and the photograph was shown in Fig. S11 and Video S4. During practical use, TENGs may suffer from huge impact of external forces, resulting in a foreseeable mechanical damage for hydrogel electrode and partial or total loss of performance for TENGs, shortening its service life. Thus, the damage immunity of the BRCH-TENG was investigated when it was subjected to destructive impact loads. As shown in Fig. 5e, a BRCH-TENG that had undergone cyclic beating (over 5000 times) was hammered hard. There was no obvious damage to the BRCH-TENG after suffering from external forces, and it maintained its initial electrical output performance (Fig. 5f). As a comparison, the H-TENG fabricated by common polyacrylamide hydrogel electrode (AAmH-TENG) occurred numerous cracks after being hammered (Fig. 5e), and the V_{oc} reduced heavily due to the damage of hydrogel electrode (Fig. S12).

The outstanding damage immunity to impact loads enables some high-impact applications for the BRCH-TENG, such as collecting mechanical energy of walking/running and detecting the motions of walking/running by assembling the BRCH-TENG under the sole of the shoe. For example, we explored the application of BRCH-TENG in walking energy harvest, human motion stride recognition and information communication (Fig. 6a). As shown in Fig. 6c, the BRCH-TENG (40 mm × 40 mm) attached to the sole of the shoe output a stable and high V_{oc} of 36 V when volunteer walked in a slow mode (the frequency is

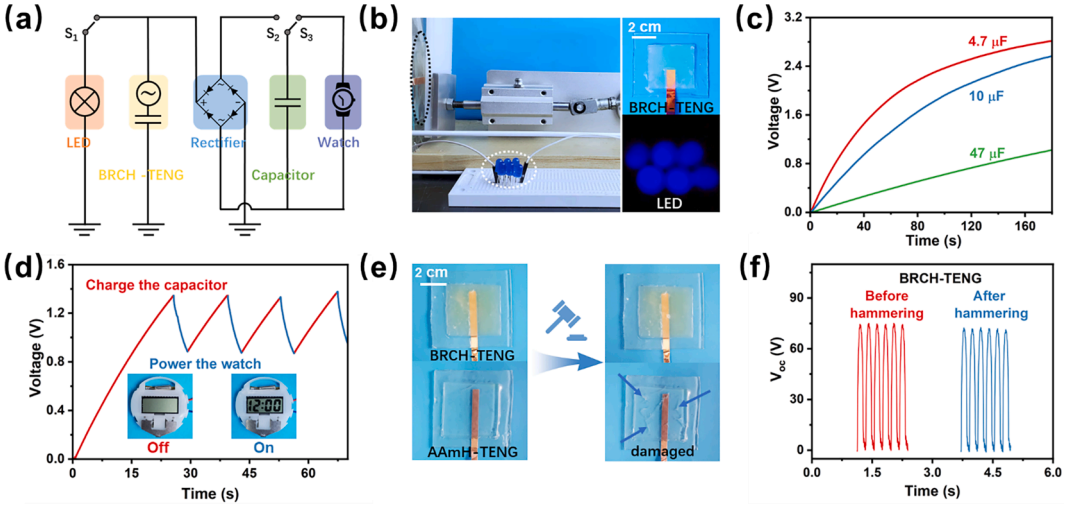

Fig. 5. The basic application of BRCH-TENG in practice. (a) The equivalent circuit of a self-charging system that uses the energy harvested from the BRCH-TENG to power electronics. (b) Photographs showing lighting 6 LEDs by tapping the BRCH-TENG. (c) Charging the capacitors with various capacitance values by tapping the BRCH-TENG. (d) Voltage profile of a 4.7 μF capacitor being charged by the BRCH-TENG and used to power an electronic watch. (e) Photographs of BRCH-TENG and AAmH-TENG before and after hammering. (f) The V_{oc} of the BRCH-TENG (40 mm × 40 mm) before and after hammering.

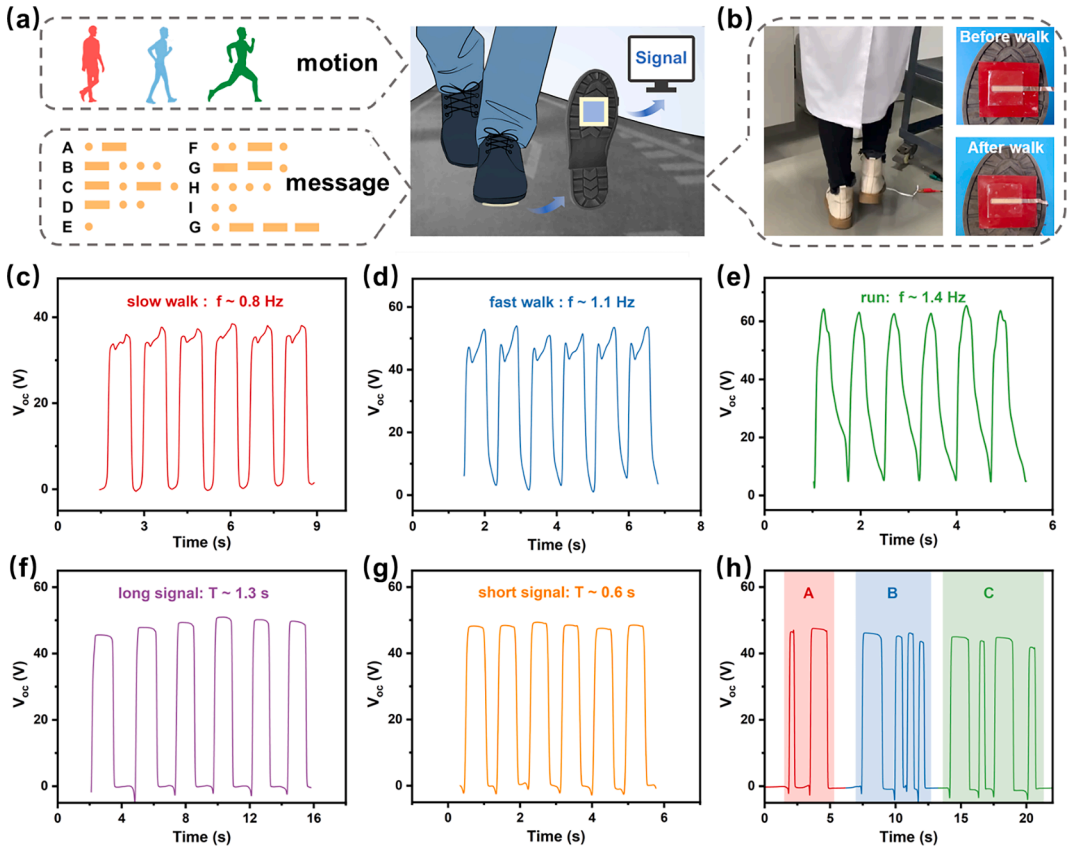

Fig. 6. Potential application for the damage-resistant BRCH-TENG in high-impact environment. (a) Illustration shows the BRCH-TENG was used to harvest walking energy, detect motion state and send information by assembling the BRCH-TENG under the sole of the shoe. (b) Photographs showing the BRCH-TENG (40 mm × 40 mm) attached to the sole of the shoe before and after walk. (c-e) V_{oc} generated by the BRCH-TENG when human (c) slow walk, (d) fast walk and (e) run. (f, g) BRCH-TENG output (f) long signal and (g) short signal by adjusting the time interval of walk. (h) Demonstration of the BRCH-TENG send a message of "ABC" through Morse code.

about 0.8 Hz). With the frequency of walk/run increased to 1.1 Hz and 1.4 Hz, the V_{oc} also increased to ~48 V and ~60 V due to the bigger impact force and greater deformation from fast walk and run (Fig. 6d and e), which is beneficial to harvesting more mechanical energy. It is worth noting that there was no any obvious damage for the BRCH-TENG after long-time repeated trampling (Fig. 6b), once again proving that the BRCH-TENG employing with the durable breakage-resistant hydrogel electrode possesses superb mechanical safety under the rapid and repeated impact of a large load. Therefore, working as a wearable self-power sensor, the BRCH-TENG exhibits great potential in human motion monitoring and posture correction (Video S5). More significantly, the BRCH-TENG attached to the sole also can be used in information encryption and communication. The holding time of the maximum V_{oc} can be controlled by adjusting the time interval of walk, and the V_{oc} can be divided into long signal and point signal as shown in Fig. 6f and g. By analogy with the mechanism of Morse code (Fig. S13), different permutations and combinations of "dots" (short-time V_{oc} signal) and "dashes" (long-time V_{oc} signal) can be used to represent different letters. As shown in Fig. 6h, as a validation, a short message of "ABC" was edited and send by rhythmically walk to communicate secretly with partner.

4. Conclusion

In summary, an eco-friendly conductive hydrogel with great breakage-resistant ability was developed by an effective enforcement method of solvent-exchange. Benefitting from the Hofmeister effect on starch polymers, there is a significant improvement in mechanical properties for the BRC hydrogel after solvent replacement by NaCit solution. Due to the formation of the bundling starch chains, the BRC hydrogel exhibits excellent modulus (~0.87 MPa), fracture energy (7.45 kJ/m^2), anti-puncture capacity (~15 MPa) and long-term stability, which ensure its mechanical reliability in case of accidental physical impact. Besides, the solvent-exchange strategy endows the hydrogel with good electrical properties by introducing free ions (Na^+, Cit^-) into the hydrogel, providing a basis for the application of electrode material in flexible TENG. Compared with the traditional TENG based on hydrogel, the BRC hydrogel based TENG not only exhibits satisfactory electrical output performances, but also possesses better mechanical safety attributed to the breakage-resistant ability of hydrogel electrode, which is crucial for TENG to prolong its service life when it suffered from destructive impact. Furthermore, the BRCH-TENG shows great potential application in the field of walking energy harvest, real-time motion state detection and information communication. The breakage-resistant hydrogel electrode is of great significance for promoting the further development of hydrogel based TENG, including improving its mechanical reliability, prolonging its service life and expanding its application areas.

Declaration of Competing Interest

The authors declare that they have no known competing financial interests or personal relationships that could have appeared to influence the work reported in this paper.

Data availability

Data will be made available on request.

Acknowledgements

This work was supported by the National Key R&D Program of China (2022YFB3200071), National Natural Science Foundation of China (52103152), China Postdoctoral Science Foundation (2021M690157; 2022T150668), Ningbo Natural Science Foundation (2121J206; 20221JCGY010301),Sino-German mobility program (M-0424) and K. C. Wong Education Foundation (GJTD-2019-13).

Appendix A. Supplementary data

Supplementary data to this article can be found online at https://doi.org/10.1016/j.cej.2022.140261.

References

[1] G. Zhu, C. Pan, W. Guo, C.-Y. Chen, Y. Zhou, R. Yu, Z.L. Wang, Triboelectric-Generator-Driven Pulse Electrodeposition for Micropatterning, Nano Lett. 12 (9) (2012) 4960–4965, https://doi.org/10.1021/nl302560k.

[2] J. Chen, Y. Huang, N. Zhang, H. Zou, R. Liu, C. Tao, X. Fan, Z.L. Wang, Micro-cable structured textile for simultaneously harvesting solar and mechanical energy, Nature Energy 1 (10) (2016) 16138, https://doi.org/10.1038/nenergy.2016.138.

[3] D.-W. Shin, M.D. Barnes, K. Walsh, D. Dimov, P. Tian, A.I.S. Neves, C.D. Wright, S. M. Yu, J.-B. Yoo, S. Russo, M.F. Craciun, A New Facile Route to Flexible and Semi-Transparent Electrodes Based on Water Exfoliated Graphene and their Single-Electrode Triboelectric Nanogenerator, Adv. Mater. 30 (39) (2018) 1802953, https://doi.org/10.1002/adma.201802953.

[4] J. Zhao, G. Zhen, G. Liu, T. Bu, W. Liu, X. Fu, P. Zhang, C. Zhang, Z.L. Wang, Remarkable merits of triboelectric nanogenerator than electromagnetic generator for harvesting small-amplitude mechanical energy, Nano Energy 61 (2019) 111–118, https://doi.org/10.1016/j.nanoen.2019.04.047.

[5] C. Jiang, X. Li, S.W.M. Lian, Y. Ying, J.S. Ho, J. Ping, Wireless Technologies for Energy Harvesting and Transmission for Ambient Self-Powered Systems, ACS Nano 15 (6) (2021) 9328–9354, https://doi.org/10.1021/acsnano.1c02819.

[6] H. Chen, Y. Song, X. Cheng, H. Zhang, Self-powered electronic skin based on the triboelectric generator, Nano Energy 56 (2019) 252–268, https://doi.org/10.1016/j.nanoen.2018.11.061.

[7] Y. Liu, J. Mo, Q. Fu, Y. Lu, N.i. Zhang, S. Wang, S. Nie, Enhancement of Triboelectric Charge Density by Chemical Functionalization, Adv. Funct. Mater. 30 (50) (2020), 2004714, https://doi.org/10.1002/adfm.202004714.

[8] Z. Liu, H. Li, B. Shi, Y. Fan, Z.L. Wang, Z. Li, Wearable and Implantable Triboelectric Nanogenerators, Adv. Funct. Mater. 29 (20) (2019) 1808820, https://doi.org/10.1002/adfm.201808820.

[9] Y. Kim, J. Yun, D. Kim, Robust and flexible triboelectric nanogenerator using non-Newtonian fluid characteristics towards smart traffic and human-motion detecting system, Nano Energy 98 (2022), 107246, https://doi.org/10.1016/j.nanoen.2022.107246.

[10] J. Yun, N. Jayababu, D. Kim, Self-powered transparent and flexible touchpad based on triboelectricity towards artificial intelligence, Nano Energy 78 (2020), 105325, https://doi.org/10.1016/j.nanoen.2020.105325.

[11] J. Luo, Z. Wang, L. Xu, A.C. Wang, K. Han, T. Jiang, Q. Lai, Y. Bai, W. Tang, F. R. Fan, Z.L. Wang, Flexible and durable wood-based triboelectric nanogenerators for self-powered sensing in athletic big data analytics, Nat. Commun. 10 (1) (2019) 5147, https://doi.org/10.1038/s41467-019-13166-6.

[12] X. He, Y. Zi, H. Yu, S.L. Zhang, J. Wang, W. Ding, H. Zou, W. Zhang, C. Lu, Z. L. Wang, An ultrathin paper-based self-powered system for portable electronics and wireless human-machine interaction, Nano Energy 39 (2017) 328–336, https://doi.org/10.1016/j.nanoen.2017.06.046.

[13] W. Zhang, L. Deng, L. Yang, P. Yang, D. Diao, P. Wang, Z.L. Wang, Multilanguage-handwriting self-powered recognition based on triboelectric nanogenerator enabled machine learning, Nano Energy 77 (2020), 105174, https://doi.org/10.1016/j.nanoen.2020.105174.

[14] S. Zhang, M. Chi, J. Mo, T. Liu, Y. Liu, Q. Fu, J. Wang, B. Luo, Y. Qin, S. Wang, S. Nie, Bioinspired asymmetric amphiphilic surface for triboelectric enhanced efficient water harvesting, Nat. Commun. 13 (1) (2022) 4168, https://doi.org/10.1038/s41467-022-31987-w.

[15] Y. Zhou, M. Shen, X. Cui, Y. Shao, L. Li, Y. Zhang, Triboelectric nanogenerator based self-powered sensor for artificial intelligence, Nano Energy 84 (2021), 105887, https://doi.org/10.1016/j.nanoen.2021.105887.

[16] S. Du, H. Suo, G. Xie, Q. Lyu, M. Mo, Z. Xie, N. Zhou, L. Zhang, J. Tao, J. Zhu, Self-powered and photothermal electronic skin patches for accelerating wound healing, Nano Energy 93 (2022), 106906, https://doi.org/10.1016/j.nanoen.2021.106906.

[17] W. Zhang, J. Zhao, C. Cai, Y. Qin, X. Meng, Y. Liu, S. Nie, Gas-Sensitive Cellulosic Triboelectric Materials for Self-Powered Ammonia Sensing, Advanced Science 9 (30) (2022) 2203428, https://doi.org/10.1002/advs.202203428.

[18] C. Zhang, W. Zhang, G. Du, Q. Fu, J. Mo, S. Nie, Superhydrophobic cellulosic triboelectric materials for distributed energy harvesting, Chemical Engineering Journal 452 (2023), 139259, https://doi.org/10.1016/j.cej.2022.139259.

[19] Z. Shao, J. Chen, K. Gao, Q. Xie, X. Xue, S. Zhou, C. Huang, L. Mi, H. Hou, A Double-Helix Metal-Chain Metal-Organic Framework as a High-Output Triboelectric Nanogenerator Material for Self-Powered Anticorrosion, Angew. Chem. Int. Ed. 61 (40) (2022) e202208994, https://doi.org/10.1002/anie.202208994.

[20] H. Park, S.-J. Oh, D. Kim, M. Kim, C. Lee, H. Joo, I. Woo, J.W. Bae, J.-H. Lee, Plasticized PVC-Gel Single Layer-Based Stretchable Triboelectric Nanogenerator for Harvesting Mechanical Energy and Tactile Sensing, Adv. Sci. 9 (22) (2022), 2201070, https://doi.org/10.1002/advs.202201070.

[21] S. Hajra, M. Sahu, A.M. Padhan, I.S. Lee, D.K. Yi, P. Alagarsamy, S.S. Nanda, H. J. Kim, A Green Metal–Organic Framework-Cyclodextrin MOF: A Novel Multifunctional Material Based Triboelectric Nanogenerator for Highly Efficient Mechanical Energy Harvesting, Adv. Funct. Mater. 31 (28) (2021), 2101829, https://doi.org/10.1002/adfm.202101829.

[22] Y. Wu, Y. Luo, T.J. Cuthbert, A.V. Shokurov, P.K. Chu, S.-P. Feng, C. Menon, Hydrogels as Soft Ionic Conductors in Flexible and Wearable Triboelectric Nanogenerators, Adv. Sci. 9 (11) (2022) 2106008, https://doi.org/10.1002/advs.202106008.

[23] Y. Qin, J. Mo, Y. Liu, S. Zhang, J. Wang, Q. Fu, S. Wang, S. Nie, Stretchable Triboelectric Self-Powered Sweat Sensor Fabricated from Self-Healing Nanocellulose Hydrogels, Adv. Funct. Mater. 32 (27) (2022), 2201846, https://doi.org/10.1002/adfm.202201846.

[24] H. Sun, Y. Zhao, S. Jiao, C. Wang, Y. Jia, K. Dai, G. Zheng, C. Liu, P. Wan, C. Shen, Environment Tolerant Conductive Nanocomposite Organohydrogels as Flexible Strain Sensors and Power Sources for Sustainable Electronics, Adv. Funct. Mater. 31 (24) (2021) 2101696, https://doi.org/10.1002/adfm.202101696.

[25] X. Luo, L. Zhu, Y.-C. Wang, J. Li, J. Nie, Z.L. Wang, A Flexible Multifunctional Triboelectric Nanogenerator Based on MXene/PVA Hydrogel, Adv. Funct. Mater. 31 (38) (2021) 2104928, https://doi.org/10.1002/adfm.202104928.

[26] B. Jiang, Y. Long, X. Pu, W. Hu, Z.L. Wang, A stretchable, harsh condition-resistant and ambient-stable hydrogel and its applications in triboelectric nanogenerator, Nano Energy 86 (2021), 106086, https://doi.org/10.1016/j.nanoen.2021.106086.

[27] Y. Wang, L. Zhang, A. Lu, Highly stretchable, transparent cellulose/PVA composite hydrogel for multiple sensing and triboelectric nanogenerators, J. Mater. Chem. A 8 (28) (2020) 13935–13941, https://doi.org/10.1039/D0TA02010A.

[28] P. Chen, Q. Wang, X. Wan, M. Yang, C. Liu, C. Xu, B. Hu, J. Feng, Z. Luo, Wireless electrical stimulation of the vagus nerves by ultrasound-responsive programmable hydrogel nanogenerators for anti-inflammatory therapy in sepsis, Nano Energy 89 (2021), 106327, https://doi.org/10.1016/j.nanoen.2021.106327.

[29] W. Xu, L.-B. Huang, M.-C. Wong, L. Chen, G. Bai, J. Hao, Environmentally Friendly Hydrogel-Based Triboelectric Nanogenerators for Versatile Energy Harvesting and Self-Powered Sensors, Adv. Energy Mater. 7 (1) (2017) 1601529, https://doi.org/10.1002/aenm.201601529.

[30] D. Yang, Y. Ni, X. Kong, S. Li, X. Chen, L. Zhang, Z.L. Wang, Self-Healing and Elastic Triboelectric Nanogenerators for Muscle Motion Monitoring and Photothermal Treatment, ACS Nano 15 (9) (2021) 14653–14661, https://doi.org/10.1021/acsnano.1c04384.

[31] Q. Guan, G. Lin, Y. Gong, J. Wang, W. Tan, D. Bao, Y. Liu, Z. You, X. Sun, Z. Wen, Y. Pan, Highly efficient self-healable and dual responsive hydrogel-based deformable triboelectric nanogenerators for wearable electronics, J. Mater. Chem. A 7 (23) (2019) 13948–13955, https://doi.org/10.1039/C9TA02711D.

[32] L. Shuai, Z.H. Guo, P. Zhang, J. Wan, X. Pu, Z.L. Wang, Stretchable, self-healing, conductive hydrogel fibers for strain sensing and triboelectric energy-harvesting smart textiles, Nano Energy 78 (2020), 105389, https://doi.org/10.1016/j.nanoen.2020.105389.

[33] V.K. Shivaraju, S.S.K. Vallayil Appukuttan, The Influence of Bound Water on the FTIR Characteristics of Starch and Starch Nanocrystals Obtained from Selected Natural Sources, Starch -, Stärke 71 (5–6) (2019) 1700026, https://doi.org/10.1002/star.201700026.

[34] İ.Y. Elbeyli, Production of crystalline boric acid and sodium citrate from borax decahydrate, Hydrometallurgy 158 (2015) 19–26, https://doi.org/10.1016/j.hydromet.2015.09.022.

[35] J.-Y. Sun, X. Zhao, W.R.K. Illeperuma, O. Chaudhuri, K.H. Oh, D.J. Mooney, J. J. Vlassak, Z. Suo, Highly stretchable and tough hydrogels, Nature 489 (7414) (2012) 133–136, https://doi.org/10.1038/nature11409.

[36] Z. Xu, F. Zhou, H. Yan, G. Gao, H. Li, R. Li, T. Chen, Anti-freezing organohydrogel triboelectric nanogenerator toward highly efficient and flexible human-machine interaction at − 30 °C, Nano Energy 90 (2021), 106614, https://doi.org/10.1016/j.nanoen.2021.106614.

[37] L.-B. Huang, X. Dai, Z. Sun, M.-C. Wong, S.-Y. Pang, J. Han, Q. Zheng, C.-H. Zhao, J. Kong, J. Hao, Environment-resisted flexible high performance triboelectric nanogenerators based on ultrafast self-healing non-drying conductive organohydrogel, Nano Energy 82 (2021), 105724, https://doi.org/10.1016/j.nanoen.2020.105724.

[38] Y. Long, Y. Chen, Y. Liu, G. Chen, W. Guo, X. Kang, X. Pu, W. Hu, Z.L. Wang, A flexible triboelectric nanogenerator based on a super-stretchable and self-healable hydrogel as the electrode, Nanoscale 12 (24) (2020) 12753–12759, https://doi.org/10.1039/D0NR02967J.

[39] L. Dong, M. Wang, J. Wu, C. Zhu, J. Shi, H. Morikawa, Stretchable, Adhesive, Self-Healable, and Conductive Hydrogel-Based Deformable Triboelectric Nanogenerator for Energy Harvesting and Human Motion Sensing, ACS Appl. Mater. Interfaces 14 (7) (2022) 9126–9137, https://doi.org/10.1021/acsami.1c23176.